ISSN 0023-1584, Kinetics and Catalysis, 2006, Vol. 47, No. 4, pp. 603–609. © MAIK "Nauka/Interperiodica" (Russia), 2006.
Original Russian Text © V.I. Zaikovskii, V.V. Chesnokov, R.A. Buyanov, 2006, published in Kinetika i Kataliz, 2006, Vol. 47, No. 4, pp. 620–626.

State of Disperse Alloy Particles Catalyzing Hydrocarbon Decomposition by the Carbide Cycle Mechanism: TEM and EDX Studies of the Cu–Ni/Al_2O_3 and Cu–Co/Al_2O_3 Catalysts

V. I. Zaikovskii, V. V. Chesnokov, and R. A. Buyanov

Boreskov Institute of Catalysis, Siberian Division, Russian Academy of Sciences, Novosibirsk, 630090 Russia
e-mail: viz@catalysis.nsk.su

Received January 10, 2005

Abstract—The state of disperse bimetallic alloy particles in the Cu–Ni/Al_2O_3 and Cu–Co/Al_2O_3 catalysts during their carbonization in butadiene-1,3 is studied by high-resolution electron microscopy and energy-dispersive X-ray analysis. During the formation of carbon nanofilaments by the carbide cycle mechanism, the catalyst is in a dissipative state such that the bimetallic particles vary in composition and have an anomalous component distribution in their bulk. The extrapolation of this state provides insight into the processes occurring in the dissipative system.

DOI: 10.1134/S0023158406040173

The development of new composites is a necessary condition for current technological progress. Very promising materials are various carbon-containing composites, including carbon fibers and nanofilaments, which are synthesized by a variety of methods. Numerous publications in this field have been devoted to the synthesis of graphite nanofilaments by the catalytic decomposition of hydrocarbons on fine particles of iron-family metals and their alloys with other metals [1].

Working in this area, we have elucidated the mechanism of carbon nanofilament formation [2–4], which is now known as the carbide cycle mechanism. In general terms, this mechanism is as follows. Different microcrystal faces of the fine metal particles play different roles in this process. The catalytic decomposition of hydrocarbons takes place primarily on specific faces called "frontal" and proceeds via the formation and decomposition of unstable carbide-like intermediates. The resulting carbon atoms dissolve in the metal bulk to produce a fairly high supersaturation and are transported by diffusion to other, "backside" faces, where the graphite phase then nucleates. Subsequently, graphite deposits with different crystallographic and morphological properties grow through the condensation of the carbon atoms.

During the growth of graphite nanofilaments, the metal particle may pass into an unordinary viscous-liquid (liquidlike) state, markedly changing its shape owing to the enhanced diffusion of atoms in its bulk [5]. For the similar processes of amorphous carbon crystallization on Ni and Fe particles, it has been demonstrated that these particles pass into the viscous-liquid state several hundreds of degrees below the metal–carbon eutectic point [6–8]. This unordinary state of metal particles has been explained in terms of the carbide cycle mechanism. It is brought about by the high diffusion flux of carbon atoms in the particle bulk, which condense on the backside face to release a large amount of energy. According to our estimates [5], the diffusion rate of carbon atoms in the bulk of a nickel particle originating a graphite nanofilament is above 600 nm/s. The transition metals Fe, Co, and Ni have a small atomic radius. In the case of Ni, whose radius is 0.124 nm, a carbon atom, whose radius is 0.077 nm, cannot fit into an octahedral hole in the fcc packing of metal atoms. Therefore, carbon atom diffusion in the nickel bulk is possible only if the metal atoms oscillate vigorously and numerous defects are produced. This "immersion" of the system of metal particles into the highly nonequilibrium conditions of the carbide cycle causes the self-organization of supramolecular structures, resulting in new dynamic states. These quasi-steady states are called dissipative. This term reflects their relation to dissipation intensity [9].

Obviously, the known equilibrium phase diagrams are inapplicable to dissipative systems consisting of two or more interacting metals. In such systems, one would expect the formation of metastable intermetallides and solid solutions, irrespective of whether they can exist under equilibrium phase-diagram conditions. In the course of some steps of the carbide cycle mechanism, there can be changes both in the values and in

the nature of the control parameters determining the stability limits of these steps. These control parameters are the composition and concentration of the hydrocarbon to be decomposed, the concentration of carbon atoms in the metal particles, hydrogen concentration on the frontal side of the particles, reaction temperature, etc. In other words, the system may show specific features caused by the variety of factors responsible for the dissipative state [9].

The realization of all carbide cycle steps forms an integrated "pattern of life" of the metal particle. Most often, it is possible to investigate only the effect produced by the dissipative system (i.e., the state of the object after the termination of the overall process). For more contrasting data, it is appropriate to study the state and distribution of a second, promoting metal in the iron-family metal particle. Knowing the state and distribution of this metal and making an inverse extrapolation, one can gain insight into the processes occurring in the dissipative system of the bimetallic particle.

Here, the following question arises: How will this dissipative system in the metal particle bulk behave if the hydrocarbon decomposition is terminated? Obviously, under new conditions, the structure of this system will relax toward the equilibrium phase diagram. However, the metal particle will pass from the viscous-liquid state to the solid state in a short time and, therefore, the relaxation processes will be suppressed.

We do not know of any attempts to observe the dissipative state of metal particles or its relaxation in the processes considered. Elucidating these points would be of both scientific and practical significance: the formation of carbon nanofilaments could be controlled more deliberately, and the synthesis could be carried out on binary and even polymetallic systems.

This work is the first attempt to answer the above questions.

EXPERIMENTAL

We studied Cu–Ni/Al_2O_3 and Cu–Co/Al_2O_3 catalysts in order to compare systems with markedly different copper solubility limits. While Cu is infinitely soluble in Ni, the solubility of Cu in Co does not exceed 10 at % in a wide temperature range [10]. The similarity between the carbon diffusion coefficients in Ni and Co does not cause any extra difficulties in data analysis.

The catalysts were prepared by the 30-min-long mechanochemical activation of three-component mixtures of metal oxides and aluminum hydroxide. The last component served as a dispersing agent. The Al_2O_3 resulting from aluminum hydroxide accounted for 10% of the total sample weight. The Cu : Ni and Cu : Co atomic ratios were always 1 : 4.

Carbon formation kinetics were studied in a quartz flow reactor with a McBain balance under zero-gradient thermal conditions. The sample weight was 0.2–0.5 g. The accuracy of weight measurements was 10^{-4} g. Before running a reaction, the catalyst was heated to 550°C within 20–30 min in flowing hydrogen. The Cu–Ni/Al_2O_3 catalyst was carbonized in butadiene-1,3 diluted with H_2 and Ar (C_4H_6 : H_2 : Ar = 1 : 20 : 75) at 450°C. Butadiene-1,3 and argon were, respectively, 99.92 and 99.97 vol % pure. Because the rate of carbon deposition on the Cu–Co/Al_2O_3 catalyst was comparatively low under these conditions, the reaction involving this catalyst was carried out at 600°C. Carbonization was terminated once the amount of deposited carbon reached ~100% of the initial catalyst weight. The state of the catalyst was stabilized by terminating the hydrocarbon decomposition reaction, cooling the sample to room temperature in an argon flow (80 l/h), and passivating the sample with oxygen (3 l/h) introduced into argon as 0.5- to 1-min-long pulses separated by 5 min. The reacted samples to be examined by electron microscopy were placed on a holey carbon film mounted on a molybdenum grid.

High-resolution TEM images were obtained on a JEM-2010 microscope with a lattice-fringe resolution of 0.14 nm at an accelerating voltage of 200 kV. Energy-dispersive X-ray (EDX) elemental analysis was carried out on an EDAX spectrometer fitted with an Si(Li) detector with a resolving power of 130 eV or better. Composition data were acquired from probed areas down to 10 nm in the two-dimensional projection of the sample on the image plane. In TEM studies, the electron probe generates characteristic X-rays throughout the sample thickness [11]. For this reason, the most definite local-composition data were obtained for the peripheral, thinnest regions of the particles. Special care was exercised to take into account the background radiation in elemental analysis, so the relative measurement error did not exceed 10%.

RESULTS AND DISCUSSION

According to TEM data, the reduced Cu–Ni/Al_2O_3 and Cu–Co/Al_2O_3 catalysts consist of aggregated Cu–Ni and Cu–Co particles. These aggregates result from the intergrowth of Cu and Ni or Co zones at the initial stage of alloying. The size of individual particles and their aggregates ranges between 5 nm and 0.5 μm. According to EDX analysis data, copper in reduced catalysts is nonuniformly distributed over particles with different sizes. These particles contain a great number of lattice imperfections such as domain boundaries and shear defects.

We have already reported the general and specific features of the growth of carbon nanofilaments on bimetallic alloy particles [1, 12, 13]. Here, we only present brief information concerning the above catalysts.

The carbonization of the Cu–Ni/Al_2O_3 catalyst yields two types of filaments. Comparatively large alloy particles have the shape of a distorted disc (flattened ellipsoid). On both of their convex sides, the

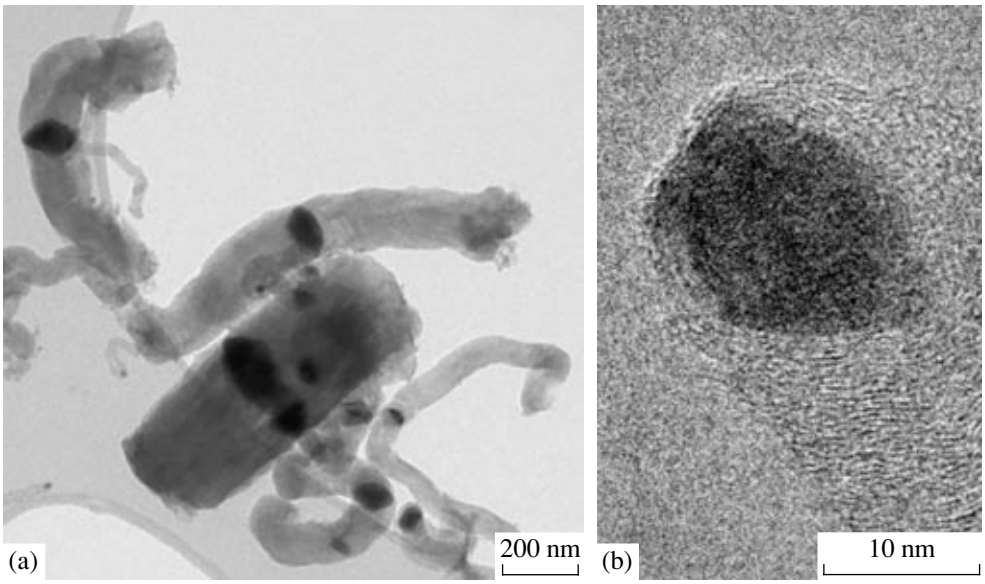

Fig. 1. Electron micrographs of the carbonized Cu–Ni/Al_2O_3 catalyst: (a) bidirectional carbon filaments containing disc-shaped Cu–Ni alloy inclusions and (b) a Cu–Ni alloy particle at the end of a unidirectional carbon filament with a coaxial-cone structure.

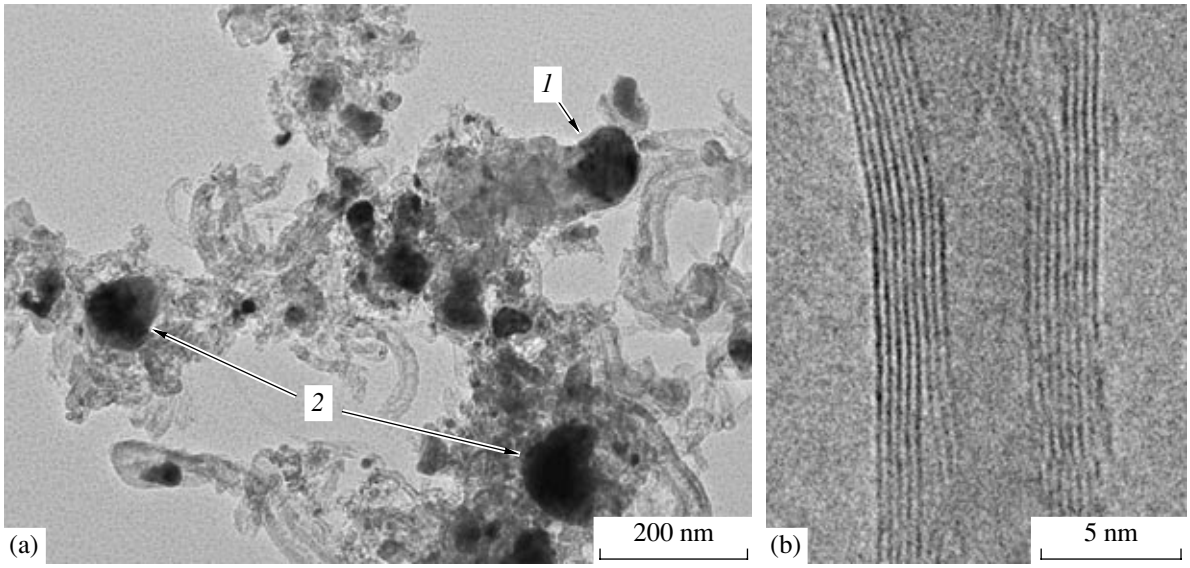

Fig. 2. Electron micrographs of the carbonized Cu–Co/Al_2O_3 catalyst: (a) Cu–Co particles and carbon as (*1*) short thick filaments and (*2*) tangled bundles of thin filaments; (b) the coaxial cylindrical structure of carbon in thin nanotubes.

longest filaments grow symmetrically, in opposite directions, as stacks of bent graphite layers (Fig. 1a). The peripheral edges of the disc-shaped particles are in contact with the gas phase. The diameter of such a particle is 50–1300 nm and is equal to the diameter of the carbon filament. The particle thickness (in the filament growth direction) is smaller by a factor of 2–5. Note that the large Cu–Ni particles are more active in carbon growth. The smallest alloy particles (10–50 nm), which assume the shape of a drop during the reaction, give birth to unidirectional short filaments consisting of coaxially nested graphite cones (Fig. 1b).

As is demonstrated in Fig. 2a, the carbonization of the Cu–Co/Al_2O_3 catalyst yields carbon as short thick filaments (*1*) or tangled bundles of thin filaments (*2*) emanating from one particle. The structure of these filaments is made up of coaxially stacked graphite cones, but it is heavily distorted. The catalyst particles in these cases are as large as hundreds of nanometers, and their shape is closer to spherical. However, the rate of carbon growth on these large Cu–Co particles is low, resulting

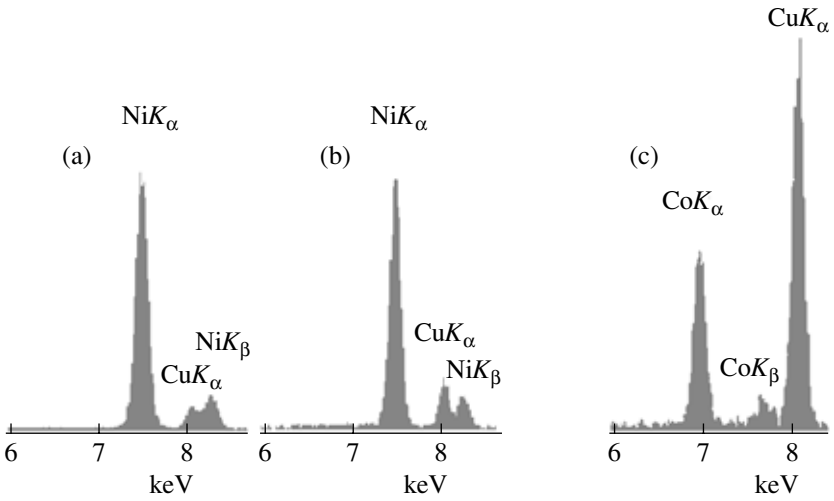

Fig. 3. EDX spectra of carbonized catalysts: (a) disc-shaped Cu–Ni particle (5 at % Cu), (b) droplike particle (17 at % Cu), and (c) selected area of a Cu–Co particle (80 at % Cu).

in short carbon filaments. The finest particles in the shape of elongated drops ~10 nm in diameter show the highest activity in the growth of carbon filaments. They give birth to long carbon filaments with a nanotube structure consisting of coaxial cylindrical graphite layers (Fig. 2b).

The above facts suggest the following inferences. First of all, note that, during the reaction, the original catalyst passes into an active state, in which the state of its particles is determined by the reaction conditions. The morphology and composition of the alloy particles are established during carbonization, when the metal phase that is active in this process (Ni or Co) is in the viscous-liquid dissipative state. In this state, the dissolution of Cu yields alloys in the intergrown regions of metal particles. Simultaneously, the alloy particles take another shape. The dependence of the morphology and crystallographic properties of the metal–carbon composites on the composition and size of the metal particles is determined by the diffusion flux of carbon atoms through the metal particle bulk during the growth of carbon nanofilaments. Here, the following obvious questions arise: What is the bimetallic system like when it is involved in the carbide cycle? And how is copper distributed in this system when it is so far from equilibrium conditions?

We have determined the elemental composition of a rather large number of catalyst particles included in various carbon filaments. Examples of EDX spectra of Cu–Ni alloy particles of various sizes are presented in Figs. 3a and 3b. It is clear from Fig. 4 that the total copper content of a Cu–Ni particle of the catalyst decreases with an increasing particle diameter. The smallest, droplike alloy particles are richer in copper than the larger, disc-shaped particles. We did not aim at striking a quantitative elemental balance. We have only determined the general trend.

The size dependence of the copper content of the Cu–Ni particles may be related to the minimization of the free surface energy of the system of particles. If this is the case, then, the smaller the particle size (i.e., the larger the surface area-to-volume ratio), the larger the amount of copper per particle weight, and, therefore, the free surface energy is lower for the size-dependent copper distribution than for the uniform copper distribution. Obviously, this can be true in view of the fact that, for particles in the unordinary viscous-liquid state, the free surface energy is lower for copper than for nickel, as in the case of thermodynamic equilibrium [14].

The composition data for the Cu–Co particles appeared to be very different. Figure 5 shows the composition versus particle size plot derived from EDX data for these particles. Clearly, the composition of the fine particles smaller than 60 nm, which are the most active in the growth of carbon filaments, is nearly constant, the copper content of the alloy being 5–8 at %. Starting at a particle diameter of 60 nm, the copper content of the Cu–Co particles increases sharply. For example, for a particle diameter of 200 nm, the copper content is ~50 at %.

No unique interpretation has been suggested for the observation that the Cu–Ni and Cu–Co systems differ in terms of the particle-size dependence of copper content. This difference may arise from the solubilities of Cu in Ni and Co being different, from the surface energies of the Cu–Ni and Cu–Co particles varying in different ways, or from Co and Ni showing different catalytic activities in the formation of carbon nanofilaments.

The most interesting and surprising data were obtained for the compositional homogeneity of alloy particles after running the carbon formation reaction. We carried out a local EDX analysis of different particle areas. The microanalysis areas and local composi-

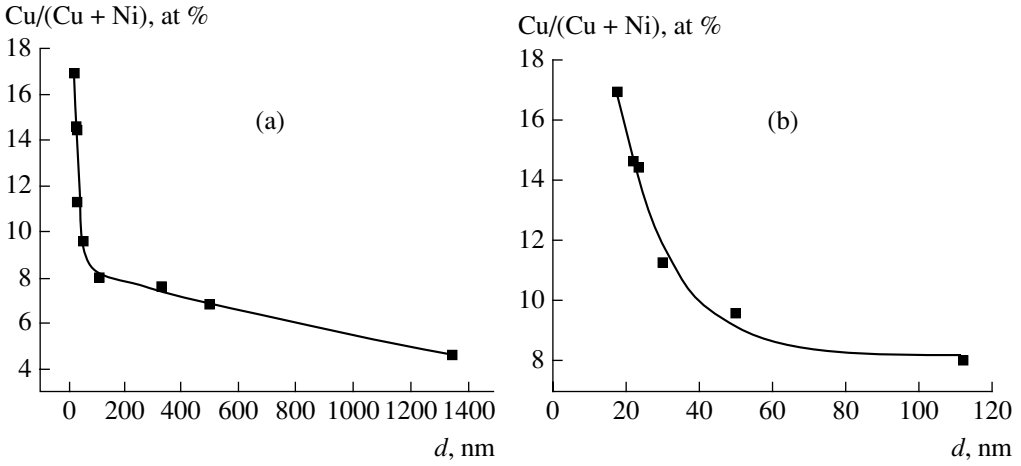

Fig. 4. Copper content of the Cu–Ni particles as a function of the particle diameter (a) in a wide diameter range and (b) for the smallest particles (<120 nm).

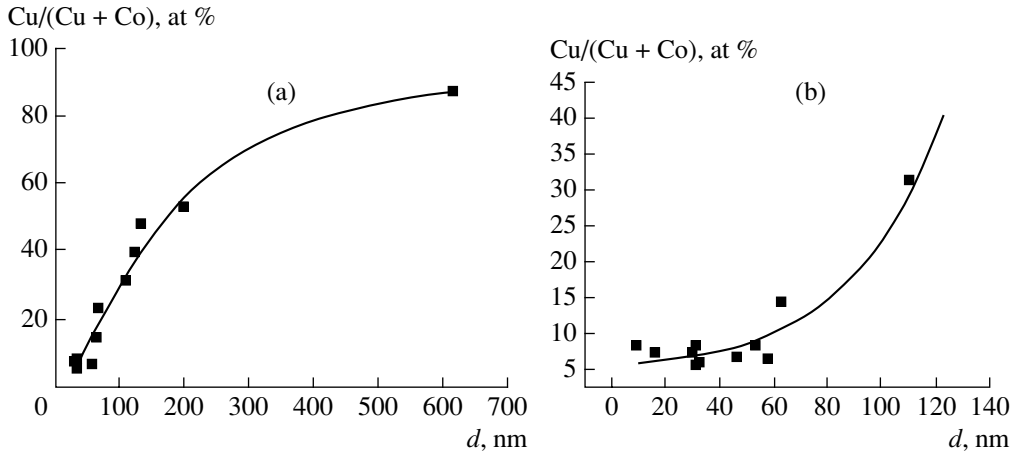

Fig. 5. Copper content of the Cu–Co particles as a function of the particle diameter (a) in a wide diameter range and (b) for the smallest particles (<120 nm).

tion data are indicated in Figs. 6 and 7. These measurements were made for bimetallic particles of all kinds observed in the carbonized Cu–Ni/Al_2O_3 and Cu–Co/Al_2O_3 catalysts.

The composition of the alloy appeared to be nonuniform even within the volume of one particle. For a disc-shaped Cu–Ni particle, the highest copper concentration is observed in its exposed part, specifically, on the disc edges exposed to the gaseous hydrocarbon. At the carbon growth sites, which are on the rear side of the particle, the copper concentration is lower by a factor up to 1.5. The copper concentration in the particle bulk is likely to be intermediate, as follows from the composition data for the middle part of the particle shown in the two-dimensional projection (Fig. 6, area *2*). This redistribution of copper between the exposed and rear parts is typical of both disc-shaped and droplike Cu–Ni particles. A still less uniform copper distribution in bimetallic particles was observed for the copper–cobalt system. Figure 7 shows a Cu–Co particle of size ~50 nm in which the local copper content decreases from 16 to 3 at % (by a factor of >5) in going from the exposed to the rear side of the particle. Note that no copper segregation yielding metal microinclusions has been detected by TEM in Cu–Ni particles of any shape and size and in Cu–Co particles smaller than 50 nm. Therefore, in these cases, copper is distributed in the particle bulk and is dissolved in Ni or Co. The contrasting stripes distinguishable in the images of typical Cu–Ni and Cu–Co particles (Figs. 6, 7) are flat twins in the defect structure of the alloy. The origin of these twins was discussed in an earlier paper [12]. EDX measurements have demonstrated that this type of defect neither gives rise to copper segregation nor affects the copper distribution in the bulk of the alloy particle. Nevertheless, in the Cu–Co particles larger than 50 nm, copper segregation does occur as separate inclusions in their bulk, as is clear from TEM images and EDX spectra. The local copper concentration in the microregions

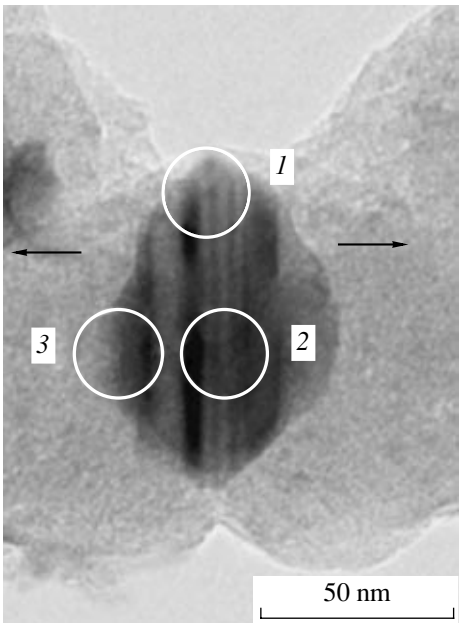

Fig. 6. Electron micrograph of the carbonized Cu–Ni/Al_2O_3 catalyst. A defective Cu–Ni alloy particle is included in a bidirectional carbon filament (the opposite growth directions are indicated by arrows). The circles show the elemental analysis areas, including (*1*) the edge of the particle (7.5 at % Cu), (*2*) the middle part of the particle (6.5 at % Cu), and (*3*) the back part of the particle (5.0 at % Cu).

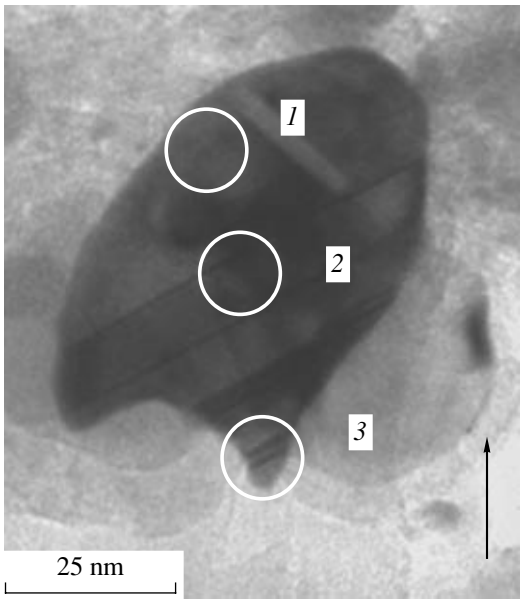

Fig. 7. Electron micrograph of the carbonized Cu–Co/Al_2O_3 catalyst. A defective Cu–Co alloy particle at the end of a carbon filament (the growth direction is indicated by an arrow). The circles show the elemental analysis areas, including (*1*) the frontal part of the particle (16.0 at % Cu), (*2*) the middle part of the particle (7.5 at % Cu), and (*3*) the back part of the particle (3.0 at % Cu).

containing copper inclusions can reach an abnormally high value of 80 at % (Fig. 3c).

The nonuniformity of the distribution of dissolved copper in the bulk of the bimetallic alloy particles, the fact that the copper concentration in the solid solution in the Cu–Co system is abnormally high as compared to the equilibrium concentration under ordinary conditions, and the appearance of separates zones with an abnormally high copper content in this system can also be explained in terms of the carbide cycle mechanism of carbon composite formation under the assumption that the bimetallic particles are in the dissipative viscous-liquid state.

Indeed, according to our notion, hydrocarbon decomposition via carbide-like compounds yields carbon atoms on the frontal side of the bimetallic particle. This gives rise to an intensive directed diffusion of carbon atoms from the particle front to the particle backside through the particle bulk. This atomic carbon has a higher active-metal (Ni or Co) affinity than Cu. Apparently, the alloy atom diffusion fluxes generated under these conditions cause the Cu atoms to move to the frontal side of the alloy particle, raising the copper concentration there. Accordingly, the Ni or Co concentration increases in the rear part of the particle and decreases in its exposed part. According to our views of the carbide cycle steps, the overall rate of carbon composite formation can be limited either by hydrocarbon decomposition on the exposed side of the particle or by the diffusion transport of carbon atoms to the rear of particle [1]. In the former case, the frontal side is somewhat depleted of active metal (Ni or Co) and this can reduce the overall process rate.

The formation of zones with an abnormally high copper content is also due to the precipitation of copper from its solution into a distinct phase after the termination of dissipation. When the bimetallic particle is in the dissipative state, the solubility limit of the promoter (in this case, Cu) in the bulk of the main component (Co) is increased to a significant extent.

Note that the extrapolation of the observed states of the bimetallic particles provides a methodological means for investigating the processes occurring in the dissipative catalytic system during carbon nanofilament formation. We admit that our interpretation of some results may be disputable. At the same time, we hope that the views presented here will contribute to the progress in this field of research.

ACKNOWLEDGMENTS

This work was supported by the Ministry of Education and Science of the Russian Federation (grant no. NSh-5469.2006.3), the Russian Foundation for Basic Research (project no. 03-03-32158), and the Division of Chemistry and Materials Science of the Russian Academy of Sciences (grant no. 4.3.1).

REFERENCES

1. Chesnokov, V.V. and Buyanov, R.A., *Usp. Khim.*, 2000, vol. 69, no. 7, p. 675.
2. Buyanov, R.A., Chesnokov, V.V., Afanas'ev, A.D., and Babenko, V.S., *Kinet. Katal.*, 1977, vol. 18, no. 5, p. 1021.
3. Buyanov, R.A., Chesnokov, V.V., and Afanas'ev, A.D., *Kinet. Katal.*, 1979, vol. 20, no. 1, p. 207.
4. Buyanov, R.A., *Zakoksovanie katalizatorov* (Coking of Catalysts), Novosibirsk: Nauka, 1983.
5. Buyanov, R.A. and Chesnokov, V.V., *Khim. Interes. Ust. Razv.*, 1995, vol. 3, no. 3, p. 177.
6. Parmon, V.N., *Catal. Lett.*, 1996, vol. 42, p. 195.
7. Gorodetskii, A.E., Evko, O.P., and Zakharov, A.P., *Fiz. Tverd. Tela*, 1976, vol. 18, p. 619.
8. Krivoruchko, O.P., Zaikovskii, V.I., and Zamaraev, K.I., *Dokl. Akad. Nauk*, 1993, vol. 329, no. 6, p. 744.
9. Glansdorff, P. and Prigogine, I., *Theory of Structure, Stability, and Fluctuations*, New York: Wiley, 1971.
10. Hansen, M. and Anderko, K., *Constitution of Binary Alloys,* New York: McGraw-Hill, 1958, 2nd ed.
11. Reimer, L., *Transmission Electron Microscopy*, Berlin: Springer, 1984.
12. Zaikovskii, V.I., Chesnokov, V.V., and Buyanov, R.A., *Kinet. Katal.*, 1999, vol. 40, no. 4, p. 612.
13. Zaikovskii, V.I., Chesnokov, V.V., Buyanov, R.A., and Plyasova, L.M., *Kinet. Katal.*, 2000, vol. 41, no. 4, p. 593.
14. Missol, W., *Energia powierzchni rozdziału faz w metalach*, Katowice: Slask, 1975.